

METHODS & TECHNIQUES

Ultra-miniature force plate for measuring triaxial forces in the micronewton range

Lars Reinhardt* and Reinhard Blickhan

ABSTRACT

Measuring the ground reaction forces of a single leg is indispensable to understanding the dynamics of legged locomotion. Because of the technical state of the art, investigations are limited to animals with a body mass above 1 g. Here we present the design, fabrication, calibration and performance of a novel ultra-miniature force platform at the micronewton level. The sensor was built using the stereolithography technology and is equipped with semiconductor strain gauges. We found a highly linear signal response in the calibrated force range to $\pm 1300 \mu\text{N}$. Individual tests revealed that our force plate still shows a linear response at forces as great as 4 mN, confirming a large measuring range and particular robustness. The sensitivity was above 50 V N^{-1} in all directions, which makes it possible to resolve forces of $10 \mu\text{N}$. We demonstrated the suitability of the device on the basis of a typical ground reaction force measurement of an ant, *Formica polyctena*.

KEY WORDS: 3D reaction force, Miniature force plate, Triaxial force measurement, Insect biomechanics, Small animal

INTRODUCTION

Ground reaction forces represent the ‘footprint’ of the dynamics of legged locomotion. Depending on the force range and the object of investigation, a number of measurement techniques are available (Table 1). Each of these is based on deformations of measuring instruments when a force is applied. Accordingly, in most cases, cantilevers equipped with strain gauges or piezo elements are used as sensing units. In the range from 1 mN up to 30 kN, three-dimensional (3D) force plates are commercially available from different manufacturers. However, for a variety of reasons, many force sensors used in biomechanical studies on small animals are custom-made. Over the last few decades, several researchers have developed two-dimensional miniature force plates for species weighing only a few grams (Heglund, 1981; Full and Tu, 1990; Drechsler and Federle, 2006; Wood et al., 2009; Lin and Trimmer, 2012). Versions of the Heglund (Heglund, 1981) force plate design were most often used to design measuring instruments for animals of different size. Furthermore, it was possible to build 3D force plates via the advancement of this design (Full et al., 1991; Katz and Gosline, 1993; Autumn et al., 2006; Dai et al., 2011). Another approach consisting of bronze springs with attached strain gauges led to a force plate within the same sensitivity range (Blickhan and Barth, 1985). Unfortunately, none of these devices are suitable to resolve 3D forces at the micronewton level. They are therefore not able to capture the dynamics of small insects, for example, in the size range of an ant.

In this area, ultrasensitive, silicon-based microelectromechanical systems (MEMS) devices seem to be the method of choice. Various prototypes and their principal usability in the field of insect biomechanics have already been demonstrated (Bartsch et al., 2007; Muntwyler et al., 2010; Kan et al., 2013). However, a major problem with these sensors is their high fragility and the associated small measuring range. Muntwyler and colleagues reported a force range for their device from ± 20 to $\pm 200 \mu\text{N}$ (Muntwyler et al., 2010). Ants are able to generate forces up to a multiple of their own weight with their mandibles. Measurements have been published showing that ants of the species *Cataglyphis fortis* could easily carry loads of 40 mg (Zollikofer, 1994). It is to be expected that these animals may generate much higher forces with their mandibles and legs, which would damage the MEMS devices.

In a first attempt, we have succeeded in building a 3D miniature force plate based on PVC springs as well as measuring ground reaction forces in ants (Reinhardt et al., 2009). This sensor combined an adequate sensitivity and robustness for our task. However, this design variant, consisting of a horizontal bar cross-connected with two orthogonally oriented bars, caused undesirable crosstalk effects. In this paper, we present a detailed description of a further development of our first prototype with significantly lower crosstalk between the channels.

RESULTS

Static calibration

Mean sensor outputs versus loading force are plotted in Fig. 1 and the corresponding values are shown in Table 2. There is a high linearity between output voltage and applied force in all directions of the sensor. Coefficients of determination (r^2) of the linear regressions were found to be nearly 1.0 for all piezoresistors. Based on these results, we determined the sensitivity matrix \mathbf{K}^{-1} :

$$\mathbf{K}^{-1} = \begin{pmatrix} -0.0978 & 0.0295 & -0.0007 \\ -0.0057 & -0.1976 & -0.0040 \\ 0.0010 & -0.0013 & -0.0510 \end{pmatrix} \text{mv} / \mu\text{N}. \quad (1)$$

Calculating the inverse of \mathbf{K}^{-1} provides the characteristic matrix \mathbf{K} :

$$\mathbf{K} = \begin{pmatrix} -10.13 & -1.51 & 0.27 \\ 0.30 & -5.02 & 0.39 \\ -0.28 & 0.13 & -19.60 \end{pmatrix} \mu\text{N} / \text{mv}. \quad (2)$$

Inserting \mathbf{K} in Eqn 13 (see Materials and methods) results in the following matrix equation:

$$\begin{pmatrix} F_x \\ F_y \\ F_z \end{pmatrix} = \begin{pmatrix} -10.13 & -1.51 & 0.27 \\ 0.30 & -5.02 & 0.39 \\ -0.28 & 0.13 & -19.60 \end{pmatrix} \begin{pmatrix} U_x \\ U_y \\ U_z \end{pmatrix}. \quad (3)$$

Science of Motion, Friedrich-Schiller-University Jena, Seidelstr. 20, 07749 Jena, Germany

*Author for correspondence (lars.reinhardt@uni-jena.de)

Received 18 July 2013; Accepted 7 November 2013

Table 1. Prior measurement techniques

Reference	Technology	Axis	Resolution
Heglund, 1981	Aluminium beams/strain gauge	2	0.1 N
Blickhan and Barth, 1985	Plastic/bronze beams/strain gauge	3	1 mN
Full and Tu, 1990	Brass beams/semiconductor strain gauge	2	1 mN
Full et al., 1991	Brass beams/semiconductor strain gauge	3	1 mN
Katz and Gosline, 1993	Brass beams/semiconductor strain gauge	3	1 mN
Drechsler and Federle, 2006	Metal beams/strain gauge	2	0.1 mN
Autumn et al., 2006	Brass beams/semiconductor strain gauge	3	0.5 mN
Bartsch et al., 2007	MEMS-based	3	1 μ N
Wood et al., 2009	Invar [®] FeNi36/capacitive sensor	2	5 μ N
Reinhardt et al., 2009	PVC-based/semiconductor strain gauge	3	10 μ N
Muntwyler et al., 2010	MEMS-based	3	1 μ N
Dai et al., 2011	Aluminium beams/strain gauge	3	1 mN
Lin and Trimmer, 2012	Acrylic/strain gauge	2	0.3 mN
Kan et al., 2013	MEMS-based	3	1 μ N

MEMS, microelectromechanical systems.

For the piezoresistors of the three directions (x , y and z), we determined the following regressions:

$$F_x(U_x) = -10.13 U_x, r^2 = 0.997, N = 40, \quad (4)$$

$$F_y(U_y) = -5.02 U_y, r^2 = 0.999, N = 40, \quad (5)$$

$$F_z(U_z) = -19.60 U_z, r^2 = 0.997, N = 25. \quad (6)$$

Matrix **K** and Fig. 1 confirm the predictions of the finite element analysis concerning the decoupling (crosstalk <2%) of the z -direction from the other two directions. Similarly, there is crosstalk below 6% in the x -direction when forces act along the y -axis. Surprisingly, we found crosstalk between F_x and F_y (see Fig. 1A). With respect to the calibrated forces, this effect is in the range of 15%. This behaviour can be corrected, because a highly significant relationship was determined through linear regression:

$$F_y(F_x) = -0.1491 F_x, r^2 = 0.988, N = 40. \quad (7)$$

Dependence on site of force application

The z -component is largely independent (<5%) of the site (± 2 mm) of force application (see Fig. 3D). As predicted by modelling, the vertically oriented bending beams changed their signals at off-centre vertical loads (Fig. 2D). Here S_x only responds to shifts of the point of

force application in the x -direction and S_y only to changes in the y -direction. In each direction, a significant ($r^2 > 0.937$) relationship between position and signal of the corresponding sensor exists. This is directly proportional to the signal of the vertical force sensor (S_z). With knowledge of S_z and the x - and y -coordinates of the point of force application, this effect could be corrected with the following equations:

$$S_x(S_z, x) = S_z(-0.3790x - 0.0371), r^2 = 0.987, N = 45, \quad (8)$$

$$S_y(S_z, y) = S_z(-0.2453y + 0.0568), r^2 = 0.937, N = 45. \quad (9)$$

One example of a static calibration experiment including force calculation under application of all corrective calculations is shown in Fig. 2.

Dynamic calibration

The dynamic calibration led to similar results as in the static experiments (Fig. 3). Because the calibration events had an average duration of 57.2 ± 8.6 ms, which is approximately equal to the contact time of an ant leg during running (see Fig. 6), these trials verify the applicability of the sensor in the field of insect biomechanics. Through the software-supported identification of the site of force application, accuracy and spatial resolution was clearly higher than in the static experiments. Accordingly, quantity and quality of the data set and thus reliability of the results were much higher.

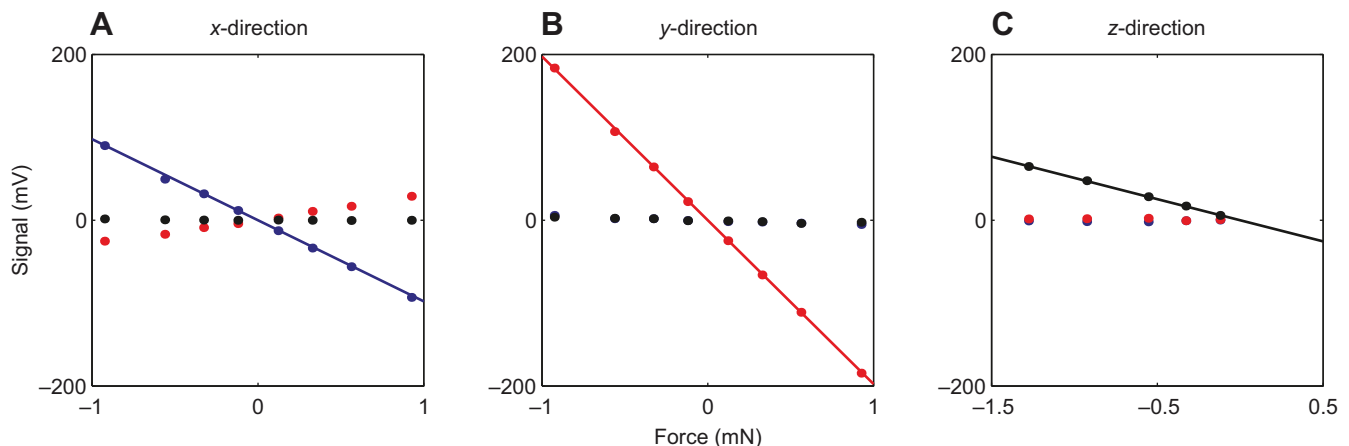


Fig. 1. Three-dimensional calibration of the force plate using standard weights between 12 and 130 mg (0.12–1.28 mN). The coloured points represent the signal changes of the strain gauges with respect to the applied load force. In each plot, the same colour scheme is used: S_x , blue; S_y , red; S_z , black. For each direction, regression lines are shown (see Eqns 4–6). As standard deviations are smaller than the marker size, no error bars are plotted (see Table 2).

Table 2. Average signal changes at different load situations

Load force (μN)	Direction (x, y, z)	U_x (mV)	U_y (mV)	U_z (mV)	N
122	1, 0, 0	-12.60 \pm 2.95	2.72 \pm 1.51	0.27 \pm 1.48	5
	-1, 0, 0	11.78 \pm 0.67	-3.98 \pm 1.13	0.10 \pm 0.92	5
328	1, 0, 0	-33.53 \pm 1.04	10.74 \pm 1.80	-0.08 \pm 0.88	5
	-1, 0, 0	31.96 \pm 1.55	-8.89 \pm 2.12	0.18 \pm 1.15	5
562	1, 0, 0	-56.07 \pm 2.68	16.96 \pm 0.84	-0.31 \pm 1.29	5
	-1, 0, 0	49.68 \pm 2.58	-16.80 \pm 1.43	0.44 \pm 1.57	5
925	1, 0, 0	-92.98 \pm 1.35	28.98 \pm 1.23	0.09 \pm 1.24	5
	-1, 0, 0	90.06 \pm 1.78	-25.14 \pm 2.02	1.66 \pm 3.43	5
122	0, 1, 0	-1.62 \pm 0.47	-24.58 \pm 1.10	-0.71 \pm 1.44	5
	0, -1, 0	-0.27 \pm 1.13	22.48 \pm 1.21	-0.53 \pm 2.31	5
328	0, 1, 0	-2.26 \pm 0.24	-65.95 \pm 0.80	-1.49 \pm 1.56	5
	0, -1, 0	1.81 \pm 1.66	64.23 \pm 1.69	1.93 \pm 1.33	5
562	0, 1, 0	-3.57 \pm 0.99	-110.89 \pm 1.97	-3.73 \pm 1.35	5
	0, -1, 0	1.92 \pm 2.88	107.08 \pm 1.27	2.40 \pm 1.29	5
925	0, 1, 0	-5.15 \pm 0.76	-184.49 \pm 1.80	-2.42 \pm 1.27	5
	0, -1, 0	5.81 \pm 2.02	183.57 \pm 2.89	3.87 \pm 2.12	5
122	0, 0, -1	0.25 \pm 0.46	0.70 \pm 0.84	5.89 \pm 0.89	5
328	0, 0, -1	-0.51 \pm 1.54	-0.46 \pm 0.40	17.08 \pm 1.18	5
554	0, 0, -1	-1.91 \pm 2.13	2.34 \pm 1.76	28.31 \pm 0.83	5
925	0, 0, -1	-1.67 \pm 0.75	1.90 \pm 0.93	47.60 \pm 1.19	5
1276	0, 0, -1	-0.92 \pm 1.96	1.58 \pm 2.77	64.81 \pm 1.81	5

Data are means \pm s.d.

Concerning the crosstalk effect at off-centre vertical loads, we determined the following equations (see Fig. 3B,C):

$$S_x(S_z, x) = S_z(-0.3690x - 0.0943), r^2 = 0.995, N = 964, \quad (10)$$

$$S_y(S_z, y) = S_z(-0.1960y - 0.1061), r^2 = 0.995, N = 820. \quad (11)$$

As soon as the steel ball was on the plate with its complete weight (322 μN), S_z remained stable at a constant level of approximately 15 mV (Fig. 3D, Fig. 4B). Consequently, the vertical calibration factor amounted to $-21.39 \pm 1.60 \mu\text{N mV}^{-1}$ and the corresponding regression equation is:

$$F_z(U_z) = -21.39 U_z, r^2 = 0.923, N = 1784. \quad (12)$$

In Fig. 4, we present one example of a dynamic experiment including force calculation under application of all corrective calculations.

Natural frequencies

Natural frequencies of the three force directions were calculated to be between 200 and 380 Hz (see Table 3). We conducted an experiment to determine the actual eigenfrequencies of the prototype. This was done by repeatedly tapping on the weighing table with approximately 5 Hz over a period of 60 s. As can be seen from Fig. 5, all significant oscillations were above 200 Hz.

Ground reaction forces in ants

One possible field of application of our miniature force plate is in research on small insects. The device has already been successfully deployed within an experimental setup for biomechanical analysis of ant locomotion. During 6 months of operation, in total approximately 1500 runs have been registered, implicating at least 3000 runs in which the platform survived without damage or

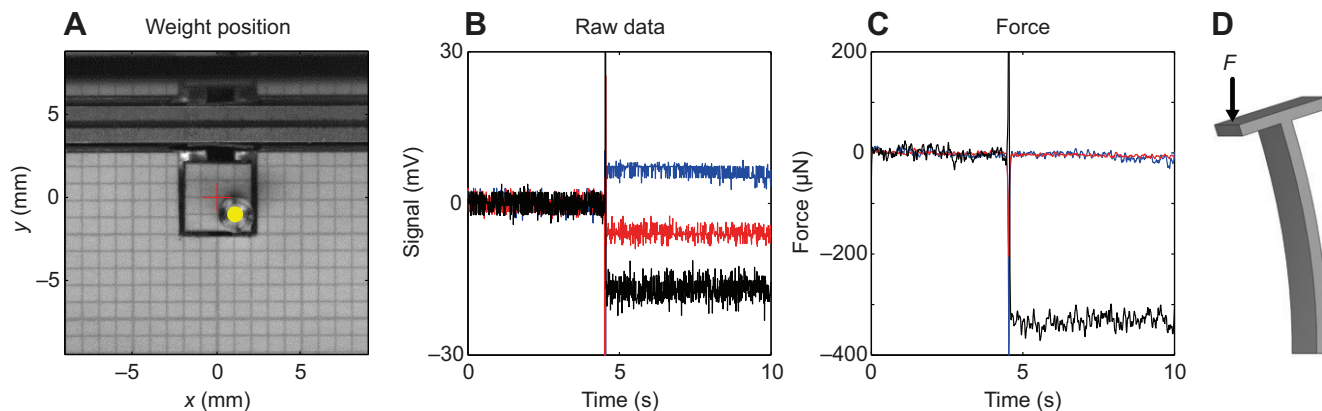


Fig. 2. Example of an off-centre calibration experiment. (A) A standard weight (yellow dot) with a mass of 33.4 mg (328 μN) was placed on the tread of the force plate at the point with the coordinates ($x=1$ mm; $y=-1$ mm) with respect to the centre of the tread (red cross). At the beginning of the measurement, a zero adjustment of all channels was performed. After approximately 5 s, the weight was carefully and quickly removed from the plate with a fine magnetic tool and the measurement was stopped after 10 s. (B) Unfiltered raw data sampled at 100 Hz (S_x , blue; S_y , red; S_z , black). Although gravitational force acted only vertically (z -direction), all channels changed their signal. These curves were low-pass (10 Hz) filtered using a first-order Butterworth filter. (C) Calculated three-dimensional forces (F_x , blue; F_y , red; F_z , black). The lateral forces superimpose at the zero level. (D) Simplified representation of the beam bending when an eccentric load is applied.

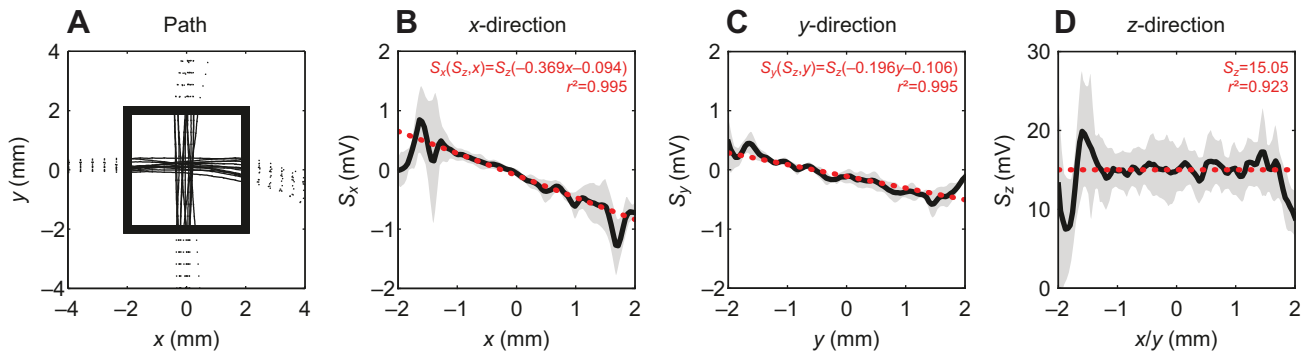


Fig. 3. Dynamic calibration using a 32.8 mg steel ball with a diameter of 2 mm. The ball was set rolling across the plate 13 times along the x-axis and just as often along the y-axis. (A) Pathways of the steel ball shown as black lines. The outline of the force plate is marked by a bold black square. (B–D) Mean signal of the strain gauges in the x- (B), y- (C) and z-directions (D) versus the position of force application. In each plot, solid black lines represent the mean values and grey areas the standard deviations. Linear regressions are designated by red dotted lines, and the equations are presented. Signals of the horizontal (x, y) channels in the plots B and C are normalised to a vertical signal of 1 mV (21.4 μ N). (D) The signal of the vertical (S_z) channel is independent from the load position and the linear regression results in a constant value.

decreased performance. One exemplary measurement of the red wood ant *Formica polyctena* is shown in Fig. 6.

DISCUSSION

In this work, we present a new design and fabrication method of a triaxial miniature force plate for the micronewton range. A 3D beam construction was built using the highly precise stereolithography (SLA) technique. The prototype was equipped with commercially available semiconductor strain gauges and connected to a digital multi-channel amplifier system. We here demonstrate that the properties of the used material are suitable for sensor design. The polycarbonate similar material is light, very elastic, well damped, and the adhesive bond with the strain gauges is solid and permanent. For the investigated range up to 1.3 mN, we found a highly linear behaviour in all directions. Furthermore, individual experiments with loads of up to 4 mN proved the same

characteristics and confirmed the particular robustness of our force plate. This property in particular is a distinct advantage compared with other highly sensitive MEMS devices described in the literature (Bartsch et al., 2007; Muntwyler et al., 2010; Kan et al., 2013). These sensors are extremely fragile and are not able to resist the maximum forces that, for instance, ants can produce with their mandibles. Thus, MEMS devices are, despite their high sensitivities, rather unsuitable for experiments with freely running insects. Additionally, they are considerably more expensive to produce. The stereolithographic manufacturing processes offer freedom of design, which makes it possible to adapt the sensor to a wide range of applications. Therefore, our measuring device can be applied far beyond the field of insect biomechanics. For example, the force plate could be invaluable to the design and testing of the next generation of micro-robots (Hoffman and Wood, 2011; Ozcan et al., 2013).

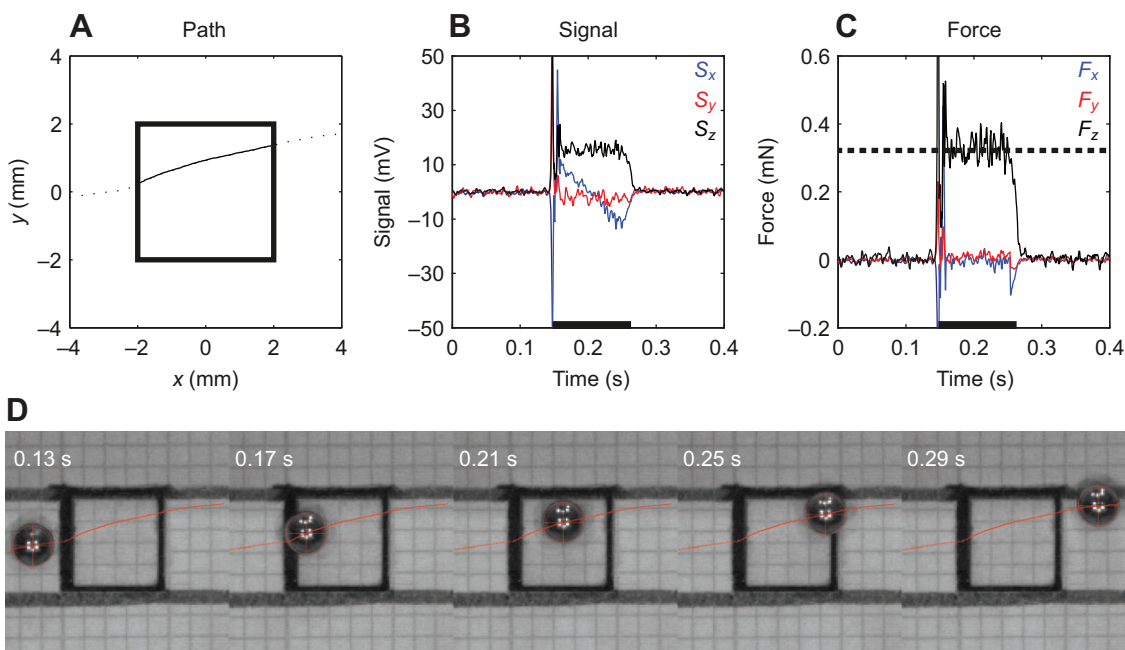


Fig. 4. Individual measurement of a rolling steel ball. Force and video data were synchronously sampled at 1200 Hz. (A) Pathway of the ball and outline of the force plate (bold square). (B) Sensor signals were smoothed by applying a low-pass first-order Butterworth filter, with a cut-off frequency of 150 Hz. A black bar on the time axis marks the stage in which the ball crossed the force plate. (C) Calculated three-dimensional forces (F_x , blue; F_y , red; F_z , black). The dotted line indicates the weight force (322 μ N). (D) Image sequence of the presented trial including the pathway (red line).

Table 3. Specification of the force plate based on finite element method (FEM) simulations and measurements

	x-direction	y-direction	z-direction
Beam dimensions (length × width × depth; mm)	10.5×4×0.4	6×4×0.5	19×4×0.4
Calculated (FEM) natural frequency (Hz)	379.16	278.93	200.77
Calculated (FEM) spring constant (N mm ⁻¹)	0.1005	0.0691	0.3598
Sensitivity (V N ⁻¹)	97.84	197.62	51.05
Unfiltered residual noise (±s.d., mV)	1.18±0.33	1.34±0.45	1.39±0.31
Resolvable force after filtering (μN)	5.42	2.87	10.75

Although in the planning phase we went to great lengths to reach low crosstalk between the individual force components, the crosstalk effect was still present. The crosstalk from the *x*- to the *y*-direction could most probably be avoided by simply positioning the strain gauge S_y higher. Although the current arrangement ensures maximum sensitivity, it also causes a relatively high transverse strain in the piezoresistor during loads in the *x*-direction. Fig. 7A shows that the lower half of S_y is placed on a stable base while the upper half is attached to the considerably more flexible beam. With the current design, eccentric vertical loads will always result in crosstalk effects. We minimize this effect by indicating the point of force application as precisely as possible so that corrective calculations can be performed subsequently. When the sensor is used, as in our case, for single leg ground reaction force measurements of small insects, this point is recorded anyway from kinematics. Another possibility is to decrease the size of the plate; however, this reduces the probability that the animals hit the plate with one leg while running. The standard method to use force distribution between four vertical channels to calculate or to compensate for the site of force application yielded unreproducible nonlinear behaviour of the vertical component. Certainly, design space is limited by size (strain gauges), mass (natural frequency) and sensitivity. Through the chosen L-shaped design, the mentioned nonlinearities are avoided and it is easily possible to arrange an array of up to four plates. This may allow us in future to measure ground reaction forces of the legs of one tripod synchronously.

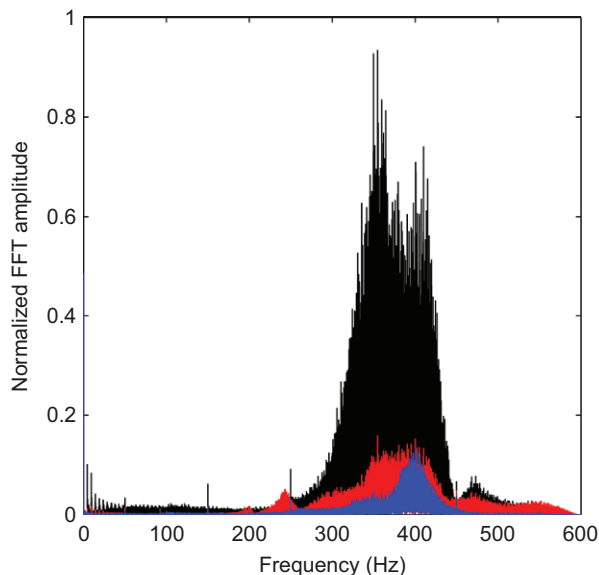


Fig. 5. Frequency spectra calculated by fast Fourier transform (FFT). The force plate was excited to oscillate by repeatedly tapping on the laboratory table with a frequency of ~5 Hz over a period of 60 s. Data were recorded at 1200 Hz and low-pass filtered at 500 Hz (Butterworth, fourth order). S_x , blue; S_y , red; S_z , black.

MATERIALS AND METHODS

Design and fabrication of the force plate

We used 3D CAD and simulation software SolidWorks 2010 (Waltham, MA, USA) to design the miniature force plate and to calculate its properties using the finite element method (FEM). The vertical (*z*) component of the sensor is composed of a parallel stack of two cantilever beam springs aligned horizontally and perpendicular to each other in a L shape (Fig. 7A). At their free ends, the springs are connected by a rigid vertical element. Perpendicularly, two additional bar springs are mounted – oriented orthogonal to each other – allowing us to register forces in the plane of movement (*x*, *y*). At the end of the upper beam, a square tread is attached. Via this element, forces can be introduced. The arrangement of two orthogonally oriented spring blade elements represents a commonly used design for two-dimensional sensors (Heglund, 1981; Klärner and Barnes, 1986; Drechsler and Federle, 2006). It ensures low crosstalk effects, is easy to manufacture and its properties are predictable by beam theory. Thus, the sensor can be adapted in advance to its later application. Our design has the advantage that the horizontal beam construction (*z*) is insensitive to loads in the *x*- and *y*-directions. Consequently, low crosstalk effects are to be expected and have been predicted by FEM (Fig. 8).

The natural frequencies were predicted to be between 200 and 380 Hz (Table 3). For fabrication, the 3D CAD model was transferred into STL format and the prototype was built layer-by-layer via SLA. In particular, the Viper si2 SLA system (3D Systems, Darmstadt, Germany) was used with a layer thickness of 0.05 mm and a material very similar to polycarbonate (Accura 60, 3D Systems, Darmstadt, Germany). At the points of the largest strain (red rectangles, Fig. 7A), each dimension was equipped with one semiconductor strain gauge of type KSP-3-120-F2-11 (Kyowa, Tokyo, Japan). For their application, a cyano-acrylate based adhesive from the same manufacturer was used (CC-33A).

Experimental setup

The sensitive unit was installed in a computer numerical control (CNC)-fabricated aluminium housing and wired with a shielded low-noise cable. We used the MGCplus data acquisition system (Hottinger Baldwin Messtechnik, Darmstadt, Germany) for signal processing. The amplifier module ML10B with an AP01i connection board was used to integrate the semiconductor strain gauges into a Wheatstone bridge circuit with a 1 V bridge excitation. No filter was chosen and the nominal value was set to 1 mV V⁻¹ for maximum gain. A desktop PC with the data acquisition software Catman Easy V3.3.3 (Hottinger Baldwin Messtechnik, Darmstadt, Germany) was connected through a USB communication processor (CP22). Raw data were saved in MDF format and all further steps of data processing were made in MATLAB R2010a (The MathWorks, Natick, MA, USA). A Fastcam SA3 high-speed video system (Photron, San Diego, CA, USA) was integrated in the setup to capture kinematics. We mounted the sensor to a vibration isolation workstation (MK2601, Minus K Technology, Inglewood, CA, USA) with a natural frequency below 1 Hz.

Static calibration

A calibration procedure is needed to evaluate a linear matrix transform (**K**, Eqn 13) between the piezoresistor bridge signals and the three-component force load vector (Valdastri et al., 2005):

$$\begin{pmatrix} F_x \\ F_y \\ F_z \end{pmatrix} = \mathbf{K} \begin{pmatrix} U_x \\ U_y \\ U_z \end{pmatrix}. \quad (13)$$

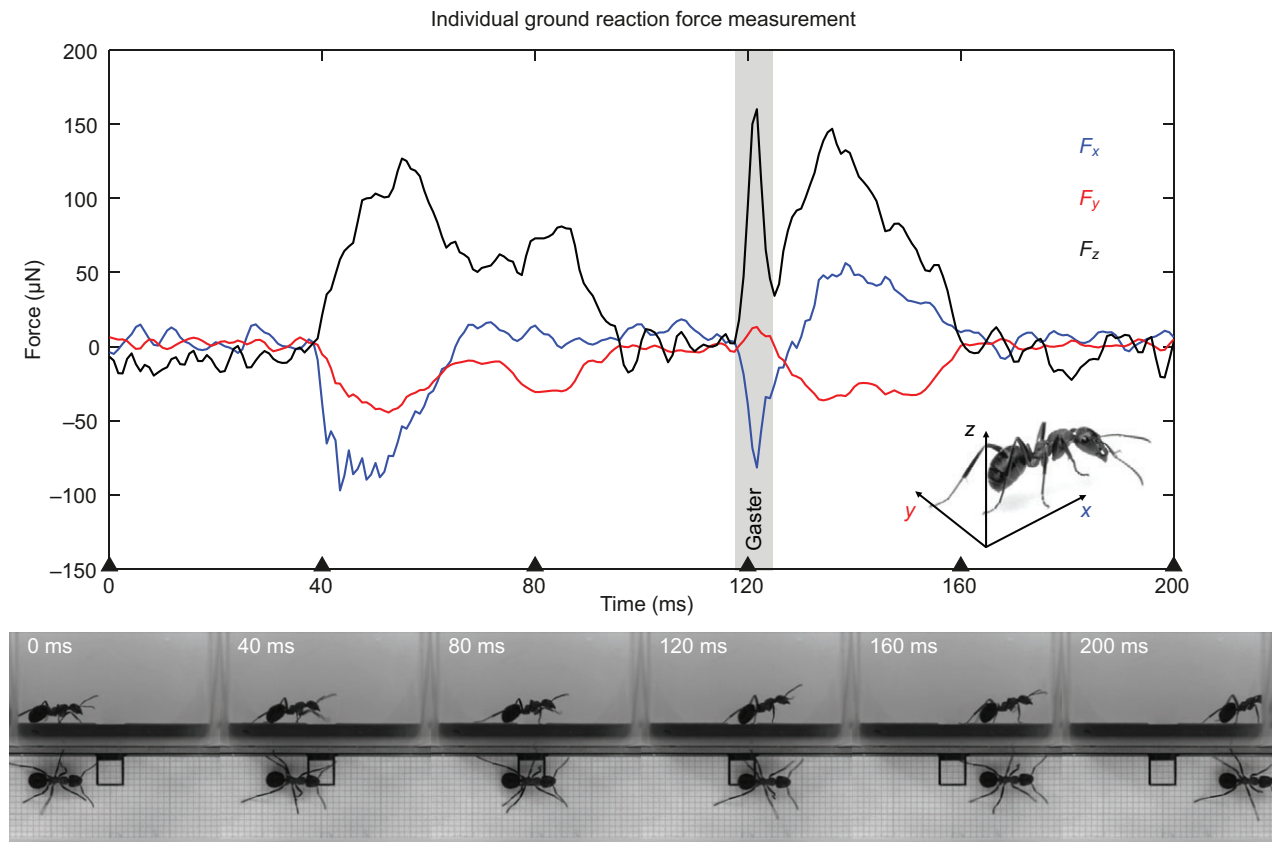


Fig. 6. Individual ground reaction force measurement of a running wood ant of the species *Formica polyctena*. Blue, fore–aft forces (F_x); red, lateral forces (F_y); black, vertical forces (F_z). The ant had a body mass of 23.2 mg and ran with a velocity of 10.2 cm s^{-1} . Force data were sampled at 1200 Hz and smoothed using a low-pass first-order Butterworth filter with a cut-off frequency of 150 Hz. An image sequence of the synchronously recorded high-speed video is shown in the lower part of the figure. The single frames are shown in a 40 ms time interval and the corresponding time points are indicated by black triangles in the force tracings. As can be seen, the ant steps on the plate firstly with the left front leg at ~40 ms. Approximately 50 ms later, the stance phase ends and the leg is lifted up again. In the horizontal force (blue) after 40 ms the ringing of this component at a frequency of ~400 Hz is observed. At ~120 ms the hind left leg steps on the tread and has ground contact until 160 ms. Closer examination of video and force registration revealed that the first major force impact at 120 ms is not generated by the hind leg but by the abdomen (gaster), which touches the ground at this instant (grey area).

To calculate K , we followed the algorithm described by Dai and colleagues (Dai et al., 2011). Five standard weights with masses from 12 to 130 mg (0.12–1.28 mN) were used and their weight was measured

accurately to 0.1 mg using an analytical balance (ABS 80-4, Kern and Sohn, Balingen, Germany). Each calibration experiment proceeded according to the same pattern. The force plate was rotated such that gravity acted in the

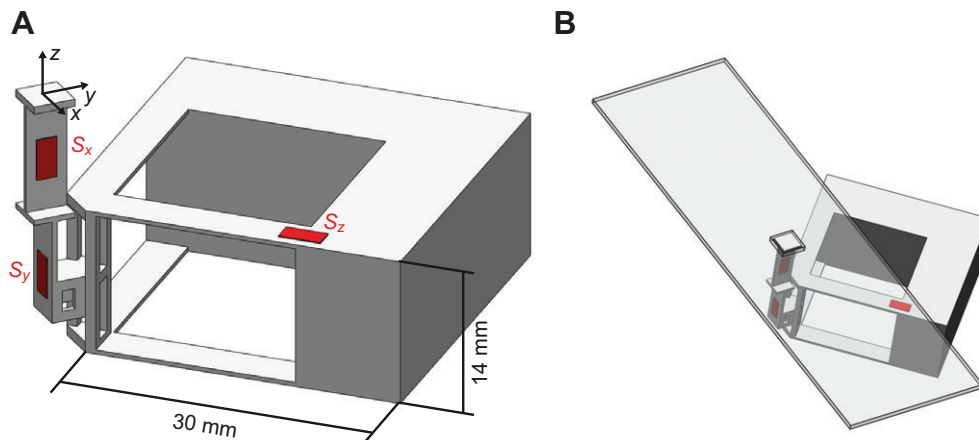


Fig. 7. Construction drawing. (A) Design of the triaxial miniature force plate. The transducer is sensitive in the three directions of the illustrated coordinate system. In each direction, at least one beam is arranged to take up the respective force component. Beam bending is measured by strain gauges whose positions are marked by red rectangles. Vertical forces (z-direction) effect bending of four horizontally aligned cantilevers. One of them is equipped with a strain gauge (S_z) at its clamping. Horizontal forces in the x- and y-directions are registered by the signal of the strain gauges S_x and S_y , respectively, on two orthogonally oriented bars. At the end of the upper beam, a square tread is attached (side length 4 mm). (B) Embedding of the force plate in our experimental runway for measuring ground reaction forces in ants.

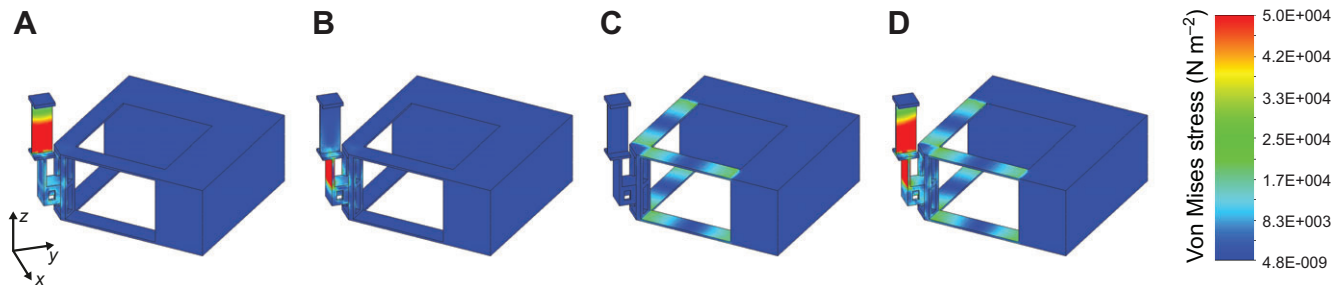


Fig. 8. Results of the finite element analysis at different load conditions. Von Mises stress in the three-dimensional model was calculated when a 1 mN force was acting on the tread in the x - (A), y - (B) and z -directions (C). A triaxial force of 1 mN in each direction causes the stress condition shown in D.

direction to be calibrated. A weight was placed on the tread, zero adjustment of all bridge channels was performed and the measurement was started. After approximately 5 s, the weight was carefully and quickly removed from the plate with a fine magnetic tool and the measurement was stopped after 10 s. This procedure was repeated five times per calibration situation. We calculated the difference between the mean voltages of the first and the last 3 s of each calibration cycle. These values were used to calculate the linear regression between the loaded weight and the output signal with the Curve Fitting Toolbox in MATLAB. Zero crossing was forced by setting up a linear equation with an intercept of zero as the regression model. From the regression analysis, the sensitivity matrix \mathbf{K}^{-1} (Eqn 14) was established, which is the inverse of \mathbf{K} :

$$\begin{pmatrix} U_x \\ U_y \\ U_z \end{pmatrix} = \mathbf{K}^{-1} \begin{pmatrix} F_x \\ F_y \\ F_z \end{pmatrix}. \quad (14)$$

Our simulations and calibration experiments have shown that the measurement of the force in the z -direction is independent from the point of force application. However, the upright-standing beams also bend at off-centre vertical loads (see Fig. 2D). To quantify this effect, we repeated the calibration process in the z -direction at nine different positions. We used scale paper bonded to the tread to define these points. They were arranged in a 3×3 matrix with a grid width of 1 mm around the centre. An example of an off-centre calibration is illustrated in Fig. 2.

Dynamic calibration

Besides the static calibration, we performed dynamic experiments using a steel ball with a mass of 32.8 mg and a diameter of 2 mm. For this, the force plate was tilted by an angle of approximately 2 deg to the plane and the steel ball was allowed to roll across the plate with a starting distance of approximately 4 cm. Because of the marginal inclination, it was assumed that only a vertical force of 322 μN acted on the sensor, when the steel ball was on the plate. The slope was chosen so that the ball rolled closely along the horizontal axes of the coordinate system (see Fig. 3A). We repeated this procedure 13 times for the x - and y -directions. The signals of the force sensor were recorded synchronously with high-speed videos at 1200 Hz (resolution: 0.077 mm pixel $^{-1}$). Steel ball kinematics were digitized using the software WINanalyze 3D (Version 2.1.1, Mikromak, Berlin, Germany). On average, the ball rolled across the plate with a velocity of 7.1 \pm 1.1 cm s $^{-1}$ (mean \pm s.d.) and the contact duration was 57.2 \pm 8.6 ms. Thus, in every single experiment, \sim 70 data points were registered to map the complete plate length of 4 mm. These data points were used to re-calculate the calibration factor in the z -direction and the crosstalk effect on S_x and S_y at off-centre vertical (z) loads.

Competing interests

The authors declare no competing financial interests.

Author contributions

L.R. made significant and substantial contributions to the conception, design, execution and interpretation of the findings being published, and drafting and revising the article. R.B. made significant and substantial contributions to the design, execution and interpretation of the findings being published.

Funding

This work was funded by the German Research Foundation (DFG) [BL 236/20-1 to R.B.].

References

- Autumn, K., Hsieh, S. T., Dudek, D. M., Chen, J., Chitaphan, C. and Full, R. J. (2006). Dynamics of geckos running vertically. *J. Exp. Biol.* **209**, 260-272.
- Bartsch, M. S., Federle, W., Full, R. J. and Kenny, T. W. (2007). A multi-axis force sensor for the study of insect biomechanics. *J. Microelectromech. Syst.* **16**, 709-718.
- Blickhan, R. and Barth, F. (1985). Strains in the exoskeleton of spiders. *J. Comp. Physiol. A* **157**, 115-147.
- Dai, Z., Wang, Z. and Ji, A. (2011). Dynamics of gecko locomotion: a force-measuring array to measure 3D reaction forces. *J. Exp. Biol.* **214**, 703-708.
- Drechsler, P. and Federle, W. (2006). Biomechanics of smooth adhesive pads in insects: influence of tarsal secretion on attachment performance. *J. Comp. Physiol. A* **192**, 1213-1222.
- Full, R. J. and Tu, M. S. (1990). Mechanics of six-legged runners. *J. Exp. Biol.* **148**, 129-146.
- Full, R. J., Blickhan, R. and Ting, L. H. (1991). Leg design in hexapedal runners. *J. Exp. Biol.* **158**, 369-390.
- Heglund, N. C. (1981). Short communication: a simple design for a force-plate to measure ground reaction forces. *J. Exp. Biol.* **93**, 333-338.
- Hoffman, K. and Wood, R. (2011). Myriapod-like ambulation of a segmented micro-robot. *Auton. Robots* **31**, 103-114.
- Kan, T., Takahashi, H., Binh-Khiem, N., Aoyama, Y., Takei, Y., Noda, K., Matsumoto, K. and Shimoyama, I. (2013). Design of a piezoresistive triaxial force sensor probe using the sidewall doping method. *J. Micromech. Microeng.* **23**, 035027.
- Katz, S. L. and Gosline, J. M. (1993). Ontogenetic scaling of jump performance in the african desert locust (*Schistocerca gregaria*). *J. Exp. Biol.* **177**, 81-111.
- Kläerner, D. and Barnes, W. J. P. (1986). The cuticular stress detector (CSD2) of the crayfish: II. Activity during walking and influences on leg coordination. *J. Exp. Biol.* **122**, 161-175.
- Lin, H.-T. and Trimmer, B. A. (2012). A new bi-axial cantilever beam design for biomechanics force measurements. *J. Biomech.* **45**, 2310-2314.
- Muntwyler, S., Beyeler, F. and Nelson, B. J. (2010). Three-axis micro-force sensor with sub-micro-Newton measurement uncertainty and tunable force range. *J. Micromech. Microeng.* **20**, 025011.
- Ozcan, O., Baisch, A. T. and Wood, R. J. (2013). Design and feedback control of a biologically-inspired miniature quadruped. IEEE/RSJ International Conference on Intelligent Robots and Systems (IROS), pp. 1438-1444. Tokyo, Japan.
- Reinhardt, L., Weihmann, T. and Blickhan, R. (2009). Dynamics and kinematics of ant locomotion: do wood ants climb on level surfaces? *J. Exp. Biol.* **212**, 2426-2435.
- Valdastri, P., Roccella, S., Beccai, L., Cattin, E., Menciassi, A., Carrozza, M. C. and Dario, P. (2005). Characterization of a novel hybrid silicon three-axial force sensor. *Sens. Actuators A Phys.* **123-124**, 249-257.
- Wood, R. J., Cho, K.-J. and Hoffman, K. (2009). A novel multi-axis force sensor for microbotics applications. *Smart Mater. Struct.* **18**, 125002.
- Zollikofer, C. (1994). Stepping patterns in ants – influence of load. *J. Exp. Biol.* **192**, 119-127.